Noninvasive Imaging of Primary Sclerosing Cholangitis: A Radiologic Perspective

13

Paul D. Russ

Abbreviations

^{18}F-FDG	Fluorodeoxyglucose
CBD	Common bile duct
CCA	Cholangiocarcinoma
CHD	Common hepatic duct
CT	Computed tomography
ERC	Endoscopic retrograde cholangiography
GBC	Gallbladder carcinoma
HCC	Hepatocellular carcinoma
IHD	Intrahepatic bile duct
kPa	Kilopascal
LSM	Liver stiffness measurement
LT	Liver transplantation
METAVIR	Meta-analysis of histological data in viral hepatitis
MRI	Magnetic resonance imaging
MRC	Magnetic resonance cholangiography
MRE	Magnetic resonance elastography
PET	Positron emission tomography
PET/CT	Positron emission tomography/computed tomography
PHTN	Portal hypertension
PSC	Primary sclerosing cholangitis
PTC	Percutaneous transhepatic cholangiography
SUV	Standardized uptake value
T1W	T1-weighted
T2W	T2-weighted
US	Transabdominal ultrasound
UTE	1-D transient elastography
VCTE™	Vibration-controlled transient elastography
VRT	Volume rendering technique

Introduction

Primary sclerosing cholangitis (PSC) is an uncommon, but nonetheless significant chronic cholestatic liver disease. It occurs in a relatively young patient population, frequently progresses to end-stage liver disease, and is highly associated with cholangiocarcinoma (CCA). Because of low disease prevalence, but frequent complications, PSC patients often receive care at institutions with advanced multidisciplinary hepatobiliary and liver transplantation services. Radiologic tests are routinely performed in the diagnosis, management, and treatment of PSC. Noninvasive modalities used include transabdominal ultrasound (US), computed tomography (CT), magnetic resonance imaging (MRI), magnetic resonance cholangiography (MRC), and positron emission tomography/computed tomography (PET/CT).

P.D. Russ, MD, FACR
Professor Emeritus, Department of Radiology, University of Colorado Hospital, University of Colorado Denver, Anschutz Medical Campus, 12605 E. 16th Ave, Aurora CO 80045, USA
e-mail: paul.russ@ucdenver.edu

L.M. Forman (ed.), *Primary Sclerosing Cholangitis*, DOI 10.1007/978-3-319-40908-5_13

Imaging of the biliary tree contributes to the diagnosis of PSC. The diagnosis of PSC is made not only from clinical history, laboratory results, and liver biopsy but also based on radiologic findings [26]. This chapter reviews the role of noninvasive imaging in PSC.

Radiologic-Pathologic Correlation

The utility of noninvasive diagnostic radiology is primarily based on the detection and demonstration of characteristic macroscopic morphologic changes of disease. By the time of presentation and diagnosis, PSC has caused macroscopic damage and morphologic alterations of the biliary tree that are relatively unique to PSC compared to other cholangiopathies. This reflects the histopathology of PSC.

PSC is a fibroinflammatory, fibroobliterative disease that nonuniformly involves the larger intrahepatic bile ducts and/or the extrahepatic bile duct. PSC causes morphologic distortion of these larger bile ducts that were initially described using percutaneous transhepatic cholangiography (PTC) and endoscopic retrograde cholangiography (ERC). The basic macroscopic finding of PSC is the presence of multiple biliary strictures separated by normal caliber or only mildly dilated bile duct segments. The nonuniformity of PSC causes asymmetries in duct morphology and disease distribution. Features of PSC as originally demonstrated by PTC and ERC include bile duct strictures, beading, mural irregularity, diverticula, pruning, focal dilatation, and duct wall thickening [4].

Of note, the normal biliary tree is difficult to demonstrate with noninvasive imaging because of its relatively small caliber. In PSC, obstructing strictures result in the upstream accumulation of bile. The increased volume of bile within at least mildly distended intra- and/or extrahepatic bile ducts results in much greater conspicuity of ducts and associated pathologic changes. Although the biophysical principles and technology of noninvasive modalities differ substantially, US, CT, MRI, and MRC all depend on contrast differences inherent in normal and pathologic tissues to generate images. Because the contrast difference between fluid bile (water) and the liver (soft tissue) is pronounced, the cholestatic pathophysiology of PSC is fundamental to its depiction.

Transabdominal Ultrasound (US)

US likely impacts the diagnosis of PSC more than it is realized. In one study, the mean age at diagnosis was 40 years [46]. The majority of PSC patients present with symptoms. The most prevalent symptom is right upper quadrant or abdominal pain. Other symptoms and signs include pruritus, jaundice, fever, and weight loss [43]. Biochemical tests are usually cholestatic, often with a disproportionately elevated alkaline phosphatase, consistent with bile duct obstruction [20]. In this clinical scenario, US is often the first test ordered, and can be the first to demonstrate the biliary tree abnormalities of PSC.

The pathophysiology of PSC contributes to its depiction at US. Inflammatory infiltration of the bile duct wall and periductal fibrosis [7, 22] results in thickening, irregularity, and increased echogenicity. Fibrosis is strongly echogenic at sonography. Superimposed obstruction can cause at least mild upstream dilatation. Fluid is anechoic at sonography. As a result, US contrast resolution is increased by the pathologic changes of PSC, and US can depict the findings of PSC (Fig. 13.1) [5, 21]. However, it should be emphasized that a negative US examination does not exclude the presence of PSC.

PSC can lead to cirrhosis and US can assess cirrhosis. Changes in hepatic shape, surface morphology, and increased parenchymal echogenicity from fibrosis can be used to suspect or establish a diagnosis of cirrhosis. Surface morphology is particularly amenable to US evaluation in the setting of perihepatic ascites, which acts as an acoustic window. Other findings of portal hypertension (PHTN) can be appreciated to include umbilical vein collaterals and splenomegaly. Spectral and color Doppler US are very useful in evaluating flow directionality and velocity, waveform morphology, and patency of hepatic vessels. Many findings at Doppler US are characteristic of cirrhosis and PHTN.

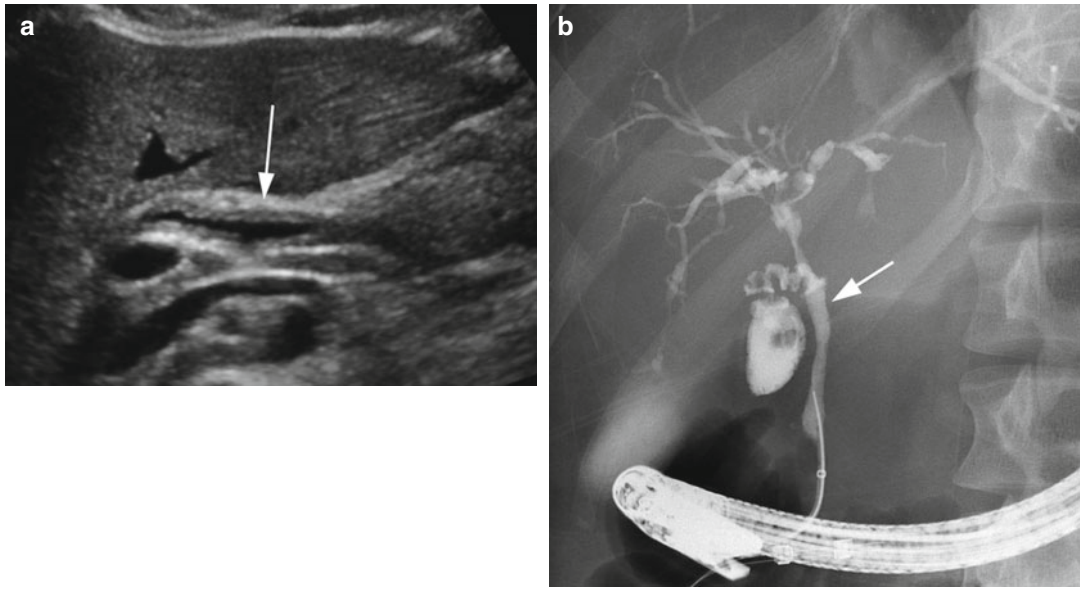

Fig. 13.1 US of a 24-year-old female with PSC. (**a**) US shows anechoic bile in mildly dilated extrahepatic bile duct, mucosal irregularity, and diffuse bile duct wall thickening (*arrow*). (**b**) Her ERC demonstrates typical luminal findings of PSC (*arrow*). Note IHD involvement

One of the most significant complications of PSC is CCA, developing in 8–14 % of PSC patients [43]. CCA can be suspected or detected by US. Intrahepatic CCAs are depicted as solid mass lesions that can be either hyperechoic or less frequently hypoechoic [32]. Intrinsic sonographic features usually do not distinguish mass-forming CCA from other intrahepatic benign or malignant neoplasms. Although the level of biliary obstruction can be correctly identified in 96 % of CCAs [31], direct demonstration of distal common bile duct (CBD) CCAs by US is limited by bowel-related gas that usually obscures the suprapancreatic and intrapancreatic CBD segments.

Perihilar CCAs (Klatskin tumors) can be demonstrated sonographically. The modified Bismuth-Corlette classification system [3] emphasizes the relationship of perihilar CCAs to the common hepatic duct (CHD). The CHD is consistently demonstrable by US. As a result, intrahepatic bile duct (IHD) obstruction to the level of the CHD is often apparent in cases of perihilar CCA [31]. Isolation of the right hepatic duct and/or left hepatic duct, nonvisualization of the CHD, abnormal CHD thickening, and abnormal soft tissue or a mass at the level of the CHD are highly suggestive of perihilar CCA, as is an associated collapsed, nondistended gallbladder in a fasting patient.

PSC patients are also at an increased risk for gallbladder carcinoma (GBC). GBC is thought to be associated with carcinogenesis induced by chronic PSC-related gallbladder inflammation and a neoplastic field effect involving the gallbladder and bile ducts [23, 30]. The prevalence of gallbladder mass lesions in PSC patients is estimated to be 3–14 % compared to 0.35 % in the general population [30]. In PSC, 56 % of mass lesions have dysplasia or are GBC. Lewis et al. pathologically evaluated 72 whole gallbladder specimens from 66 cholecystectomies performed at liver transplantation (LT) and 6 cholecystectomies performed prior to LT in PSC patients [23]. GBC was found in 14 % of the gallbladders. In addition, gallbladder intestinal metaplasia, low-grade dysplasia, and high-grade dysplasia were identified as significant associated risk factors. A metaplasia-flat dysplasia-carcinoma sequence was proposed for GBC in PSC patients.

US is the best modality to evaluate the gallbladder. Because of the risk of GBC in PSC, both the American Association for the Study of Liver

Diseases (AASLD) and the European Association for the Study of the Liver (EASL) recommend annual abdominal ultrasound for the detection of gallbladder lesions [30]. It is recommended that cholecystectomy be performed for all polyps ≥0.8 cm and probably for all polyps < 0.8 cm, unless the patient is a very poor cholecystectomy candidate, in which case the lesion should be sonographically reevaluated every 3–6 months.

Computed Tomography (CT)

CT is a readily available noninvasive imaging modality with significant impact in PSC. Current multi-detector scanners generate images with high spatial resolution and high temporal resolution. High spatial resolution results from thin slices (~1 mm) and fast acquisition speed. Thin slices increase image sharpness and anatomic detail. Thin slices allow for the postprocessing of data sets using multiplanar reformatting (MPR), maximum intensity projection (MIP), and volume rendering techniques (VRT). These postprocessing algorithms produce nonaxial images displayed in coronal, sagittal, and nonorthogonal projections. VRT images can be rotated and tumbled in contiguous conventional and nonconventional projections for optimal anatomic display. For surgical planning, advanced software and an independent 3-D workstation can be used for lobar and segmental volumetrics and to display the anatomy of the hepatic veins, portal vein, and hepatic artery. High temporal resolution allows for bolus tracking of exogenously administered contrast with segmented time frames of image acquisition used to generate arterial, portal venous, and delayed phases of enhancement. Unfortunately, CT cholangiography with positive-contrast excretion into the bile ducts can no longer be performed. The contrast material used, Cholografin®, is no longer available in the United States.

Analogous to US, CT is often performed in patients with abdominal pain and jaundice. It is not uncommon for CT to be the first test to detect PSC. The CT findings of PSC, especially early in its course, can be subtle. Mildly dilated IHDs have a disconnected "dot-dash" pattern corresponding to end-on and longitudinally oriented distended duct segments separated by intervening soft tissue density strictures [42]. Even small, peripheral IHDs can be conspicuous within the background liver, being filled with low-density bile, which intrinsically increases the otherwise moderate contrast resolution of CT. The fibroinflammatory and fibroobliterative changes of PSC manifest as duct wall thickening, irregularity, and narrowing, with the degree of duct wall enhancement being variable and inconsistent [38]. Mural changes are most apparent at the level of the CHD. By CT, the CHD is large enough to be consistently demonstrated in patients without or with PSC. Low-density fat in the hepatic hilum delineates its outer wall, and low-density bile within the CHD lumen defines its inner wall. The CHD is discernible as a ring-like structure on axial images and is normally of uniform thickness ≤1.5 mm. In PSC, the CHD becomes irregular with wall thickening potentially ≥2.0 mm (Fig. 13.2) [38].

Fig. 13.2 CT of a 37-year-old female with PSC. CT shows common hepatic duct dilatation with intraluminal bile, wall thickening, and bile duct wall enhancement (*arrow*)

CCA can be suspected or detected by CT. Intrahepatic CCA can present as a mass lesion. Intrahepatic CCAs do have neovascularity. In larger intrahepatic CCAs, macroscopic neovascularity tends to be sparse, stringy, and peripheral. Mass-forming intrahepatic CCAs tend to be dominated by an abundant, central fibrous stroma with scant tumor cellularity. At

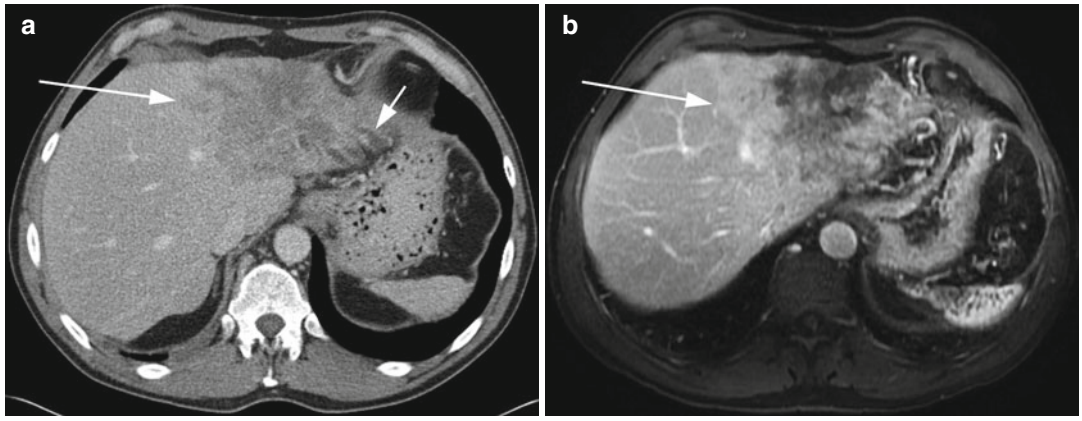

Fig. 13.3 Cholangiocarcinoma in a 52-year-old male with PSC. (**a**) Portal venous phase CT depicts a large, poorly marginated, heterogeneous intrahepatic mass-forming cholangiocarcinoma (*long arrow*) in the left hepatic lobe associated with obstructed peripheral bile ducts (*short arrow*). (**b**) Intrahepatic mass-forming cholangiocarcinoma in same patient demonstrated by portal venous phase MRI (*arrow*)

arterial phase CT, these CCAs tend to have no discernible to mild peripheral enhancement with central iso- to hypodensity. During the portal venous and delayed phases, there can be centripetal enhancement with contrast retention in the extracellular matrix of the central fibrous tissue, which can be subtle [14]. These lesions tend to be rounded, somewhat poorly marginated in non-cirrhotic livers, but pseudoencapsulated in cirrhosis; they can be associated with overlying capsular retraction, adjacent dilated IHDs, and satellite nodules (Fig. 13.3a) [10, 37, 39]. With intrahepatic mass-forming CCAs, vascular encasement is common, but macroscopic thrombus is unusual [10]. The features of intrahepatic CCA can overlap with those of hepatocellular carcinoma (HCC), particularly poorly differentiated HCCs or larger HCCs with central necrosis.

Small intrahepatic CCAs can appear as arterial phase hypervascular nodules [8, 9]. These CCAs tend to accumulate contrast, and enhance during the portal venous and delayed phases of multiphasic imaging. This is compared to typical small HCCs which wash out and become hypodense during the portal venous and delayed phases. However, arterial phase hypervascular CCAs with subsequent washout do occur.

PSC patients with cirrhosis are at an increased risk of HCC, which is estimated to be up to 2% per year [30]. This is probably related to the association of HCC and cirrhosis. Given the overlap of imaging features, HCC should be considered in PSC patients with cirrhosis.

Of perihilar CCAs, 70% are of the periductal infiltrating morphologic subtype [14]. These can be difficult to demonstrate by CT and can appear only as a stricture. Although some features such as duct wall thickening >5 mm, stricture length ≥18–22 mm, shouldering, portal venous or delayed phase enhancement, and soft tissue stranding within portal fat planes suggest perihilar periductal infiltrating CCA, these findings are insufficient to reliably differentiate dominant benign strictures from malignant strictures in PSC [14, 38]. Of note, malignant lymphadenopathy is common in cases of perihilar infiltrating CCA [14].

Of perihilar CCAs, 12–22% are of the mass-forming morphologic subtype [14]. Perihilar masses measuring 1–9 cm can occur with features analogous to intrahepatic mass-forming CCAs. Small lesions can be seen as hypervascular arterial phase nodules. Larger lesions tend to have less pronounced arterial phase rim enhancement and can have portal venous or delayed phase washin and contrast retention within the central fibrous stroma. Portal vein invasion with visible thrombus can be seen.

Distal CCAs are anatomically defined as involving the CBD between the cystic duct origin

and the ampulla of Vater [29]. Approximately 89 % are periductal infiltrating, and 11 % are intraductal growing [19]. CBD dilatation is present in 96 % of cases. Imaging findings are usually limited to CBD dilatation with abrupt downstream narrowing, irregular wall thickening, and enhancement. Because these lesions tend not to be mass forming, only 11 % have associated main pancreatic duct dilatation. Main pancreatic duct dilatation occurs when the tumor extends into the downstream ampulla of Vater or into the surrounding pancreatic parenchyma [19].

Magnetic Resonance Imaging (MRI)

Dynamic multiphasic abdominal MRI with an exogenous intravascular-extracellular contrast agent provides anatomic and enhancement characterization of PSC and its complications that are analogous to CT. An advantage of MRI is better contrast resolution compared to CT. A disadvantage of MRI is decreased spatial and temporal resolution compared to CT. Decreased spatial resolution and increased noise from physiological motion is also worse with MRI because of its relatively slower data acquisition time compared to CT. However, because of the differences in image content, CT and MRI are unpredictably complementary, and both are often used in cases of PSC.

Noncontrast MRI is used to generate two fundamentally different types of images. T2-weighted (T2W) images are based on differences in the micromagnetic environment of water-associated protons in fluid versus solid tissue. T2W MRI displays fluid as markedly hyperintense compared to an intermediate to hypointense soft tissue background. T1-weighted (T1W) images are derived from differences in the macromolecular environment of water-associated protons in fluid versus soft tissue. Using T1W MRI, fluid appears hypointense compared to mild to moderately hyperintense soft tissue. Because T1W images can be acquired faster, spatial resolution is better than with T2W scanning.

The inherently high contrast resolution of MRI can be augmented by intravenously administered exogenous contrast material. With the exception of hepatobiliary-specific agents, the pharmacokinetics of gadolinium-based MRI contrast is equivalent to iodinated CT contrast material. Intravenously administered gadolinium-based MRI contrast, which is not hepatobiliary specific, is used to generate a multiphasic dynamic series of T1W images that are analogous to multiphasic dynamic CT. Gadolinium-based agents increase the contrast resolution and signal-to-noise ratio, improving spatial resolution and lesion conspicuity. Because of its intravascular-extracellular distribution, gadolinium contrast demonstrates the same enhancement features of focal and diffuse pathology and of normal background anatomic structures as does iodinated CT contrast. As a result, a dynamic multiphasic T1W MRI series can be generated with arterial, portal venous, and delayed phases, with hypervascular lesions appearing hyperintense and hypovascular lesions being hypointense. With routine MRI scanning protocols, gadolinium contrast does not produce clinically significant changes in T2W images; postcontrast T2W scans are not obtained.

Using conventional contrast-enhanced MRI, the depicted features of PSC and its complications are the same as with CT (Fig. 13.3b). With multiphasic T1W MRI, the bile duct changes of PSC are shown as wall irregularity, thickening, and enhancement. Biliary obstruction is shown as duct dilatation accentuated by retained intraluminal bile that remains hypointense to the liver. Intrahepatic or perihilar mass-forming CCA can show arterial phase rim enhancement with centripetal washin during the portal venous and delayed phases. On T2W images, biliary obstruction is shown as duct dilatation accentuated by retained intraluminal bile that is hyperintense to the liver. Mass-forming CCA tends to be mild to moderately hyperintense compared to background hepatic parenchyma on T2W scans.

Magnetic Resonance Cholangiography (MRC)

The initial detection and diagnosis of PSC by US, CT, and MRI are usually limited to previously undiagnosed patients presenting with unexplained

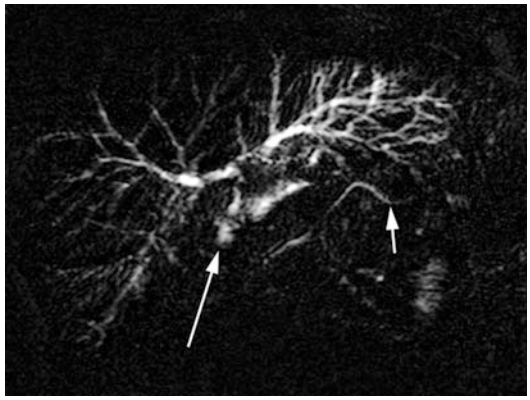

Fig. 13.4 Recurrent PSC in an allograft of a 59-year-old male, 7 years after LT with Roux-en-Y anastomosis for PSC. MRC shows recurrent PSC in the allograft. Note fluid in the Roux loop (*long arrow*). Incidentally, main pancreatic duct segment demonstrated (*short arrow*)

abdominal pain and jaundice. When PSC and/or its complications are clinically suspected or established, MRC becomes an important noninvasive imaging modality. MRC is a heavily T2W MRI technique that generates high signal intensity from fluid bile. The intrinsic T2W hyperintensity of bile outlines the luminal morphology of normal and abnormal bile ducts against such an extremely hypointense background that solid tissue becomes indiscernible. Several sets of MRC images are acquired using different parameters to optimally demonstrate the biliary tree. Data sets can be directly obtained or indirectly produced by postprocessing in any anatomic plane for display. Directly acquired thick-slab coronal images with multiple obliquities around the sagittal axis and high resolution 3-D images reconstructed with postprocessing into a coronal rotational VRT data set result in images that are equivalent to invasive positive-contrast cholangiography (ERC and PTC). The multiprojectional and rotational features of MRC are optimal for the display of significant bile duct findings that could otherwise be obscured by the overlap of structures.

The MRC findings of PSC are the same as those described for ERC and PTC (Fig. 13.4) [25, 45]. Dave et al. reported a meta-analysis of the diagnostic performance of MRC compared to ERC and PTC [13]. Studies were selected only if they included a control group of patients with other hepatobiliary diseases. Of the manuscripts that fulfilled criteria for analysis, the overall prevalence of PSC among the study patients was 185/456 (41 %). MRC interpretations were compared to ERC or PTC as the reference standards. MRC had results comparable to conventional cholangiography with a sensitivity in detecting PSC of 86 % and a specificity of 94 %. In addition, three clinical scenarios were simulated to evaluate the impact of pretest probability on the results. When the pretest probability of PSC was 25 % (low clinical suspicion), the posttest probability of PSC given a negative MRC was 5 % (considered sufficient to exclude PSC). When the pretest probability was 75 % (high clinical suspicion), the posttest probability of PSC given a positive MRC was 98 % (considered sufficient to diagnose PSC). In what was considered the worst-case scenario, a pretest probability of 50 %, the posttest probability of PSC given a positive MRC was 94 %, and the posttest probability of PSC given a negative MRC was 13 %. MRC can be quickly performed in conjunction with dynamic multiphasic MRI providing additive information in cases of PSC and its complications [27, 34, 37].

In a retrospective study of 64 PSC patients, Ruiz et al. suggested that MRC features combined with multiphasic liver MRI findings can be used to predict PSC disease progression [34]. All patients had at least two MRCs separated by at least a 1-year interval with multiple scans performed in some patients. A semiquantitative method was used to systematically score both MRI and MRC findings to assess PSC disease severity. Scores from the first and last MRI and MRC were compared, with an interval increase in score considered disease worsening, no score change considered disease stability, and a decrease in score to be considered improvement. At mean follow-up of 4 years (range, 1–9), 58 % showed radiologic worsening, 42 % remained stable, and no patient showed improvement. Using data derived from the subgroup with interval worsening, two MRI progression risk score equations were developed, one for studies performed without contrast and another for studies performed with contrast. It was noted that nearly 90 % of patients with radiologic worsening had

an elevated progression risk score, compared to a low progression risk score in nearly 85 % of patients with stable disease. In addition, over the study interval, 5/64 (8 %) patients were diagnosed with PSC-associated malignancies, CCA ($n=2$), GBC ($n=2$), and HCC ($n=1$). Ruiz et al. concluded that risk score analysis could predict PSC disease progression and suggested that annual MRI and MRC were useful for PSC surveillance [34].

The MRC findings of PSC-related CCA are the same as those described for ERC and PTC, viz., a dominant stricture with malignant features. Compared to benign strictures, malignant strictures tend to be longer (≥18–22 mm) with asymmetric narrowing, irregular margins, and shouldering [14]. These findings, however, are relatively nonspecific. Irregular margins and asymmetric narrowing are found in 30 % of benign strictures. Gradual tapering and abrupt narrowing are seen equally in benign and malignant strictures. The most common cholangiographic finding in PSC-related CCA is progressive stricture formation with increased upstream bile duct dilatation [37]. Low-risk, noninvasive serial MRC is particularly suitable for detecting progressive stricture formation [34]. Although useful for detecting suspicious findings and providing a roadmap for subsequent ERC, MRC cannot replace ERC for brush cytology or therapeutic interventions such as stenting. It is important to note, however, that noninvasive imaging should be performed before interventional procedures to avoid postprocedural changes, pneumobilia, and stent-associated artifact that can and do degrade radiologic results.

MR Elastography (MRE)

Morbidity and mortality from biliary cirrhosis, PHTN, and liver failure affect a large proportion of PSC patients [43, 46]. As reported by Wiesner et al., among a group of 174 PSC patients, liver biopsy showed septal fibrosis (Stage 3) or cirrhosis (Stage 4) in 43 % of asymptomatic patients and in 69 % of symptomatic patients [46]. During a mean follow-up of 5.2 years, 22 % of initially asymptomatic PSC patients developed liver failure. During a mean follow-up of 6.2 years, 49 % of symptomatic patients developed liver failure or died, with 93 % of deaths attributable to liver disease; 9 % of symptomatic patients were referred for or underwent LT. Therefore, monitoring the development and progression of hepatic fibrosis/cirrhosis in PSC has a significant impact on patient management.

Elastography is now used to quantitatively measure liver stiffness, a surrogate biomarker for hepatic fibrosis/cirrhosis in lieu of subjective cross-sectional imaging assessment and/or liver biopsy [41]. Elastography can be performed using either US or MRE. A commonly used US implementation is 1-D transient elastography (UTE). FibroScan® uses UTE with proprietary technology termed vibration-controlled transient elastography (VCTE™) [28]. A US probe is used to intermittently deliver compression waves to a region of interest in the right hepatic lobe with a volume 100 times larger than liver biopsy. Within the hepatic parenchyma, compression waves generate shear waves based on the viscoelastic properties of the liver tissue. Shear wave speed increases with liver stiffness, which increases with hepatic fibrosis. The ultrasound transducer tracks and measures shear wave velocity in meters per second, which is then converted into a liver stiffness measurement (LSM) expressed in kilopascals (kPa). In a cohort of 73 PSC patients who underwent liver biopsy, Corpechot et al. verified that a METAVIR-derived histologic fibrosis score correlated with VCTE LSMs [11]. Values predictive of fibrosis stages ≥F1, ≥F2, ≥F3, and F4 were 7.4 kPa, 8.6 kPa, 9.6 kPa, and 14.4 kPa, respectively.

Commercially available FDA-approved proprietary MRE technology is currently manufactured by Resoundant, Inc. It can be implemented as an upgrade on currently available MRI scanners manufactured by GE Healthcare, Philips Healthcare, and Siemens Healthcare [41]. An external flexible membrane attached to the right upper quadrant is used to generate continuous compression waves that are converted to shear waves within the liver [12, 41, 44]. Intrahepatic shear waves are tracked and displayed as axial maps of the liver at four separate slice locations; color-coded MR elastograms are used to generate results reported as shear stiffness in kilopascals

(kPa) [41]. It should be noted that UTE and MRE use different algorithms to quantify liver stiffness. The liver stiffness measurement by UTE in kPa is not equivalent to the shear stiffness measurement by MRE in kPa; the UTE value is numerically three-times larger than the MRE value [17].

Huwart et al. verified that the histologic METAVIR fibrosis scoring system correlated with MRE measurements of shear elasticity in a cohort of 96 consecutive patients who underwent liver biopsy for suspected chronic liver disease [17]. Values predictive of fibrosis stages ≥F1, ≥F2, ≥F3, and F4 were 2.4 kPa, 2.5 kPa, 3.1 kPa, and 4.3 kPa, respectively. MRE needs to be verified in a cohort of PSC patients.

Some studies suggest that MRE has performance characteristics that exceed those of UTE and other sonographic methodologies [12, 18, 41]. Machine time for MRE data acquisition is 1–2 min; MRE can be performed along with routine dynamic MRI and MRC. The technical success rate of MRE is significantly higher than UTE (94 % vs. 84 %, $P=0.016$) [18]. MRE can be accurately performed in patients with ascites and obesity. UTE cannot be used when there is perihepatic ascites because shear waves do not propagate through liquids. A 4.5 % UTE failure rate (no LSM value obtainable) correlates with a body mass index >28 kg/m^2 [16]. When correlated with histology, using area under receiver operating characteristic curve analysis to compare predictive performance, MRE was significantly better than UTE for METAVIR fibrosis stages F ≥1, F ≥2, F ≥3, and F=4 among a heterogeneous group of chronic liver disease patients [18]. It is suggested that the increased accuracy of MRE is related to the large tissue volume and the noncontiguity of the four 10-mm-thick cross sections through the liver, which reduces sampling error introduced by inhomogeneously distributed fibrosis [40].

Positron Emission Tomography/ Computed Tomography (PET/CT)

PET/CT is a noninvasive imaging modality that coregisters the results of a whole-body PET scan with CT. PET is a nuclear medicine study that is most commonly performed using the radionuclide fluorodeoxyglucose, ^{18}F-FDG, to map the cellular metabolism of glucose. Inflammation and malignant growth increases the uptake and retention of intracellular ^{18}F-FDG. The radioactive decay of ^{18}F-FDG is used to generate a scan of differential metabolic activity. Relative differences in radioactivity are semiquantitatively measured as a function of standardized uptake value (SUV), and hypermetabolic foci are displayed as areas of increased saturation on a color map. With PET/CT, the PET color map is superimposed or fused onto images from a conventional CT performed sequentially before or after the PET acquisition to colocalize the areas of increased metabolism to anatomic structures.

In PSC patients, PET/CT can be used in primary tumor (CCA) detection, but is more often incorporated into the staging of patients who are being considered for tumor resection or LT. Annunziata et al. recently published a meta-analysis of ^{18}F-FDG PET alone or PET/CT in the evaluation of the primary tumor in cases of suspected or documented intrahepatic, perihilar, and distal CCA in a spectrum of patients [2]. Both PET alone and PET/CT were shown to be accurate in the diagnosis of primary CCA. For PET/CT, overall sensitivity and specificity in the detection of primary CCA was 82 % and 75 %, respectively. For the detection of hilar CCA, using either PET or PET/CT, sensitivity and specificity were 84 % and 95 %, respectively. However, the authors noted that additional studies were needed to verify the findings in perihilar CCA, given the small number of cases in the meta-analysis.

Alkhawaldeh et al. reported the ^{18}F-FDG PET/CT results of a PSC cohort, 47/65 (72 %) with CCA [1]. Using semiquantitative SUV analysis, sensitivity and specificity for primary tumor detection were 94 % and 83 %, respectively. There were six false-positive studies, four from inflammatory strictures of PSC and two related to stent placement.

Li et al. reported on the utility of ^{18}F-FDG PET/CT in the preoperative staging of 17 patients, with perihilar CCA (background liver disease if present not specified), who underwent exploratory laparotomy with the intent of radical

resection [24]. Histologic confirmation of primary tumor, regional lymphadenopathy, and distant metastases was available in all cases. The sensitivity of whole-body PET/CT in detecting the primary perihilar CCA was 58.8 %.

As noted by Ruys et al., data regarding the role of ^{18}F-FDG PET/CT in detecting malignant locoregional lymphadenopathy and distant metastases is sparse [36]. In the study by Li et al., the sensitivity and specificity in detecting lymph node metastases were 41.7 % and 80 %, respectively, with PET-avid malignant nodes ranging in size from 4 to 30 mm [24]. For distant metastases involving the liver and peritoneum, sensitivity and specificity were 55.6 % and 87.5 %, respectively.

Presurgical Staging of Cholangiocarcinoma

There are two potentially curative surgical options for de novo and PSC-related CCA, radical resection and LT [33]. Noninvasive imaging is especially important in perihilar CCA because tumor involvement of the bile ducts, hepatic artery, and portal vein at the hepatic hilum determines resectability, and radial tumor diameter ≤3 cm is required for LT. Imaging is also used to evaluate for locoregional lymphadenopathy and distant metastases.

As noted by Ruys et al., published data describing the diagnostic performance of CT, MRI, US, and PET/CT for the preoperative staging of perihilar CCA is limited [36]. CT was found to be the most frequently used radiologic test. Meta-analysis was not feasible for MRI, US, or PET/CT because of the small number of patients in the data sets. Abstracted results for longitudinal ductal involvement, portal vein involvement, hepatic artery involvement, lymph node metastases, and distant metastases are presented in Table 13.1 [36].

In the staging of perihilar CCA, CT is usually performed because of its high spatial resolution, anatomic detail, and temporal resolution. Primary tumor radial diameter, longitudinal ductal extension, portal vein involvement, and hepatic artery involvement can be evaluated. Given their high contrast resolution, MRI and MRC can provide complementary information to CT results with regard to tumor size, hilar/perihilar extension, and bile duct involvement, but MRI usually has poorer spatial and temporal resolution of the hepatic artery and the portal vein, which can be worsened by MRI flow-related artifact.

The accuracy of CT is limited in the evaluation of locoregional nodes in perihilar CCA. The meta-analysis by Ruys et al. yielded a summary estimate of 61 % sensitivity and 88 % specificity for detecting metastatic lymphadenopathy [36]. In routine CT interpretation, a short-axis diameter >10 mm is used to define metastatic nodal enlargement. However, in a pathologic study of resected nodes in perihilar CCA, Ruys et al. noted 65 % sensitivity and 61 % specificity for nodal positivity using a cutoff value of 10.5 mm [35]. In one study, PET/CT had 41.7 % sensitivity

Table 13.1 Diagnostic performance values for CT, MRI, US, and PET/CT in the preoperative staging of perihilar cholangiocarcinoma [36]

	Accuracy (%)	Sensitivity (%), specificity (%)			
	Bile duct	Portal vein	Hepatic artery	Lymph node	Distant
CT[a]	86	89, 92	84, 93	61, 88	67, 94[c]
MRI[b]	71–80	79, 0[c]	–	–	–
US[b]	59–82	75–83, 93–100	0–43, 100	–	–
PET/CT[b]	–	–	–	42, 80[c]	56, 88[c]

– no data, *Bile duct* longitudinal bile duct extension, *portal vein* portal vein involvement, *hepatic artery* hepatic artery involvement, *lymph node* lymph node metastases, *distant* distant metastases

[a]Summary estimates except for distant metastases

[b]Non-pooled ranges

[c]Single study

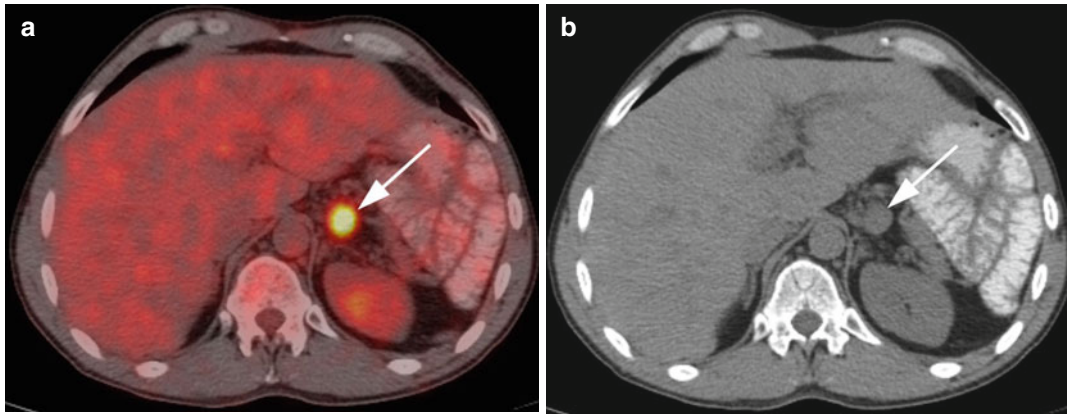

Fig. 13.5 ^{18}F-FDG PET/CT in a 45-year-old male with PSC. (**a**) Markedly PET-avid nonmalignant, reactive gastrohepatic lymph node (*arrow*) depicted by fused PET/CT. (**b**) Concurrent CT scan without intravenous contrast shows the enlarged node (*arrow*). This node decreased in size during 7 years of follow-up imaging

and 80 % specificity in detecting malignant lymphadenopathy [24]. Limited results are usually attributed to the high prevalence of PSC inflammatory lymphadenopathy (Fig. 13.5) [35]. Therefore, lymph node sampling by staging laparoscopy or laparotomy is performed prior to definitive surgery [14, 33].

Extranodal metastases to the liver, peritoneum, lung, adrenal glands, and bones occur in perihilar CCA [14]. Because multiphasic liver CT can be incorporated into a complete CT examination of the chest, abdomen, and pelvis, CT is useful to screen for distant metastases. In one study, CT had a 67 % sensitivity and 94 % specificity for detecting distant metastases [15]. In one study, PET/CT had a 56 % sensitivity and 88 % specificity in demonstrating distant metastases [24]. However, in both of these studies, the evaluation of distant metastatic disease was limited to the liver and peritoneum. Although staging laparoscopy or laparotomy is important to diagnose peritoneal carcinomatosis, laparoscopy and laparotomy are limited to evaluating metastatic disease within the abdomen. Complete CT of the chest, abdomen, and pelvis or whole-body PET/CT (usual coverage from calvarial vertex through the upper thighs) could show extra-abdominal disease in the noninvasive preoperative staging of patients with perihilar CCA. In addition, there is evidence that ^{18}F-FDG PET/CT is accurate in detecting bone metastases and is superior to conventional whole-body bone scintigraphy, especially in the axial skeleton [6].

Conclusion

US, CT, MRI, MRC, and PET/CT are noninvasive radiologic tests used in the care of patients with PSC and its complications. All of these modalities can depict the findings of PSC. Any could be the first exam to detect PSC in subclinical cases. In established cases of PSC, US is used to annually screen PSC patients because of their high risk for gallbladder adenocarcinoma.

MRC is accurate in the diagnosis of PSC. MRC findings parallel those of ERC, with potentially better display of intrahepatic bile duct changes. Because MRC is noninvasive and does not involve the use of ionizing radiation, its utility for surveillance of disease progression and PSC-related complications is being recognized. However, the demonstration of a dominant stricture by MRC still requires follow-up ERC for therapeutic management and for evaluation of malignancy.

CT remains the noninvasive radiologic workhorse in patients with an established diagnosis of PSC. It is used to evaluate cholangitis (e.g., cholangitic abscess formation), deteriorating liver function, fibrosis/cirrhosis, PHTN, and malignancy (CCA, HCC, or GBC). Important in tumor staging, CT helps to char-

acterize the primary malignancy with regard to size, radial and longitudinal spread, invasion of the hepatic artery and portal vein, associated bile duct dilatation, and involvement of contiguous structures such as the hepatoduodenal ligament and duodenum [14, 15, 36]. Although limited in assessing malignant lymphadenopathy and peritoneal carcinomatosis, multiphasic dynamic liver CT performed in conjunction with CT of the chest, abdomen, and pelvis can be used to screen for distant metastases.

PET/CT can provide additional information in PSC, especially in cases complicated by malignancy. Although the data is limited, PET/CT can contribute to the detection of the primary tumor, malignant lymph nodes, and distant metastases. False-positive results associated with the fibroinflammation and reactive lymphadenopathy of PSC are noted as a potential limitation (Fig. 13.5).

Among the more investigative technologies, MRE is the most likely to be incorporated next into the routine evaluation of PSC patients. Quickly performed along with MRI and MRC, MRE can accurately quantitate fibrosis in both hepatic lobes. Because MRE is noninvasive, unlike liver biopsy, potentially more accurate than liver biopsy and sonographic elastography, and does not use ionizing radiation, MRE could become the study of choice to evaluate hepatic fibrosis, progression of hepatic fibrosis, and response to evolving antifibrotic therapies.

In summary, US, CT, MRI, MRC, and PET/CT are routinely used in the care of PSC patients. Each modality is unique. None demonstrate all of the findings of PSC and its complications. Depending on the clinical situation, the judicious use of more than one of these complementary studies is likely to provide the most complete information for the best care of PSC patients.

References

1. Alkhawaldeh K, Faltten S, Biersack HJ, Ezziddin S. The value of F-18 FDG PET in patients with primary sclerosing cholangitis and cholangiocarcinoma using visual and semiquantitative analysis. Clin Nucl Med. 2011;36:879–83.
2. Annunziata S, Caldarella C, Pizzuto DA, Galiandro F, Sadeghi R, Giovanella L, et al. Diagnostic accuracy of fluorine-18-fluorodeoxyglucose positron emission tomography in the evaluation of the primary tumor in patients with cholangiocarcinoma: a meta-analysis. Biomed Res Int. 2014;2014:247693. doi:10.1155/2014/247693. Epub 2014 May 13.
3. Bismuth H, Nakache R, Diamond T. Management strategies in resection for hilar cholangiocarcinoma. Ann Surg. 1992;215:31–8.
4. Campbell WL, Ferris JV, Holbert BL, Thaete FL, Baron RL. Biliary tract carcinoma complicating primary sclerosing cholangitis: evaluation with CT, cholangiography, US and MR imaging. Radiology. 1998;207:41–50.
5. Carroll BA, Oppenheimer DA. Sclerosing cholangitis: sonographic demonstration of bile duct wall thickening. AJR Am J Roentgenol. 1982;139:1016–8.
6. Chang CY, Gill CM, Simeone FJ, Taneja AK, Huang AJ, Torriani M, et al. Comparison of the diagnostic accuracy of 99 m-Tc-MDP bone scintigraphy and 18 F-FDG PET/CT for the detection of skeletal metastases. Acta Radiol. 2016;57(1):58–65. doi:10.1177/0284185114564438.
7. Chapman RWG, Arborgh BAM, Rhodes JM, Summerfield JA, Dick R, Scheuer PJ, et al. Primary sclerosing cholangitis: a review of its clinical features, cholangiography, and hepatic histology. Gut. 1980;21:870–7.
8. Choi JY, Lee JM, Sirlin CB. CT and MR imaging diagnosis and staging of hepatocellular carcinoma: part I. Development, growth, and spread: key pathologic and imaging aspects. Radiology. 2014;272:635–54.
9. Choi JY, Lee JM, Sirlin CB. CT and MR imaging diagnosis and staging of hepatocellular carcinoma: part II. Extracellular agents, hepatobiliary agents, and ancillary imaging features. Radiology. 2014;273:30–50.
10. Chung YE, Kim MJ, Park YN, Choi JY, Pyo JY, Kim YC, et al. Varying appearances of cholangiocarcinoma: radiologic-pathologic correlation. Radiographics. 2009;29:683–700.
11. Corpechot C, Gaouar F, Naggar AE, Kemgang A, Wendum D, Poupon R, et al. Baseline values and changes in liver stiffness measured by transient elastography are associated with severity of fibrosis and outcomes of patients with primary sclerosing cholangitis. Gastroenterology. 2014;146:970–9.
12. Cui J, Heba E, Hernandez C, Haufe W, Hooker J, Andre MP, et al. MRE is superior to ARFI for the diagnosis of fibrosis in patients with biopsy-proven NAFLD: a prospective study. Hepatology. 2016;63(2):453–61. doi:10.1002/hep.28337.
13. Dave M, Elmunzer BJ, Dwamena BA, Higgins PDR. Primary sclerosing cholangitis: meta-analysis of diagnostic performance of MR cholangiopancreatography. Radiology. 2010;256:387–96.
14. Engelbrecht MR, Katz SS, van Gulik TM, Lameris JS, van Delden OM. Imaging of perihilar cholangiocarcinoma. AJR Am J Roentgenol. 2015;204:782–91.

15. Engels JT, Balfe DM, Lee JKT. Biliary carcinoma: CT evaluation of extrahepatic spread. Radiology. 1989; 172:35–40.
16. Foucher J, Castera L, Bernard PH, Adhoute X, Laharie D, Bertet J, et al. Prevalence and factors associated with failure of liver stiffness measurement using FibroScan in a prospective study of 2114 examinations. Eur J Gastroenterol Hepatol. 2006;18:411–2.
17. Huwart L, Sempoux C, Salameh N, Jamart J, Annet L, Sinkus R, et al. Liver fibrosis: noninvasive assessment with MR elastography versus aspartate aminotransferase-to-platelet ratio index. Radiology. 2007;245:458–66.
18. Huwart L, Sempoux C, Vicaut E, Salameh N, Annet L, Danse E, et al. Magnetic resonance elastography for the noninvasive staging of liver fibrosis. Gastroenterology. 2008;135:32–40.
19. Kim JH, Kim MJ, Chung JJ, Lee WJ, Yoo HS, Lee JT. Differential diagnosis of periampullary carcinomas at MR imaging. Radiographics. 2002;22:1335–52.
20. Krones E, Graziadei I, Trauner M, Fickert P. Evolving concepts in primary sclerosing cholangitis. Liver Int. 2012;32:352–69.
21. Laing FC, Jeffrey Jr RB, Wing VW, Nyberg DA. Biliary dilatation: defining the level and cause by real-time US. Radiology. 1986;160:39–42.
22. Lee YM, Kaplan MM. Primary sclerosing cholangitis. N Engl J Med. 1995;332:924–33.
23. Lewis JT, Talwalkar JA, Rosen CB, Smyrk TC, Abraham SC. Prevalence and risk factors for gallbladder neoplasia in patients with primary sclerosing cholangitis: evidence for a metaplasia-dysplasia-carcinoma sequence. Am J Surg Pathol. 2007;31:907–13.
24. Li J, Kuehl H, Grabellus F, Muller SP, Radunz S, Antoch G, et al. Preoperative assessment of hilar cholangiocarcinoma by dual-modality PET/CT. J Surg Oncol. 2008;98:438–43.
25. MacCarty RL, LaRusso NF, Wiesner RH, Ludwig J. Primary sclerosing cholangitis: findings on cholangiography and pancreatography. Radiology. 1983;149: 39–44.
26. Nakanuma Y, Zen Y, Portmann BC. Diseases of the bile ducts. In: Burt AD, Portmann BC, Ferrell LD, editors. MacSween's pathology of the liver. Edinburgh: Churchill Livingstone/Elsevier; 2012. p. 491–562.
27. Park HS, Lee JM, Choi JY, Lee MW, Kim HJ, Han JK, et al. Preoperative evaluation of bile duct cancer: MRI combined with MR cholangiopancreatography versus MDCT with direct cholangiography. AJR Am J Roentgenol. 2008;190:396–405.
28. Patel K, Wilder J. Fibroscan. Clin Liver Dis. 2014;4: 97–100.
29. Razumilava N, Gores GJ. Cholangiocarcinoma. Lancet. 2014;383:2168–79.
30. Razumilava N, Gores GJ, Lindor KD. Cancer surveillance in patients with primary sclerosing cholangitis. Hepatology. 2011;54:1842–52.
31. Robledo R, Muro A, Prieto ML. Extrahepatic bile duct carcinoma: US characteristics and accuracy in demonstration of tumors. Radiology. 1996;198: 869–73.
32. Ros PR, Buck JL, Goodman ZD, Ros AM, Olmsted WW. Intrahepatic cholangiocarcinoma: radiologic-pathologic correlation. Radiology. 1988;167:689–93.
33. Rosen CB, Heimbach JK, Gores GJ. Liver transplantation for cholangiocarcinoma. Transpl Int. 2010;23: 692–7.
34. Ruiz A, Lemoinne S, Carrat F, Corpechot C, Chazouilleres O, Arrive L. Radiologic course of primary sclerosing cholangitis: assessment by three-dimensional magnetic resonance cholangiography and predictive features of progression. Hepatology. 2014;59:242–50.
35. Ruys AT, Kate FJ, Busch OR, Engelbrecht MR, Gouma DJ, van Gulik TM. Metastatic lymph nodes in hilar cholangiocarcinoma: does size matter? HPB (Oxford). 2011;13:881–6.
36. Ruys AT, van Beem BE, Engelbrecht MRW, Bipat S, Stoker J, van Gulik TM. Radiological staging in patients with hilar cholangiocarcinoma: a systematic review and meta-analysis. Br J Radiol. 2012;85: 1255–62.
37. Sainani NI, Catalano OA, Holalkere NS, Zhu AX, Hahn PF, Sahani DV. Cholangiocarcinoma: current and novel imaging techniques. Radiographics. 2008;28:1263–87.
38. Schulte SJ, Baron RL, Teefey SA, Rohrmann Jr CA, Freeny PC, Shuman WP. CT of the extrahepatic bile ducts: wall thickness and contrast enhancement in normal and abnormal ducts. AJR Am J Roentgenol. 1990;154:79–85.
39. Soyer P, Bluemke DA, Reichle R, Calhoun PS, Bliss DF, Scherrer A, et al. Imaging of intrahepatic cholangiocarcinoma: 1. peripheral cholangiocarcinoma. AJR Am J Roentgenol. 1995;165:1427–31.
40. Talwalkar JA. Elastography for detecting hepatic fibrosis: options and considerations. Gastroenterology. 2008;135:299–302.
41. Tang A, Cloutier G, Szeverenyi NM, Sirlin CB. Ultrasound elastography and MR elastography for assessing liver fibrosis: part I, principles and techniques. AJR Am J Roentgenol. 2015;205:22–32.
42. Teefey SA, Baron RL, Rohrmann CA, Shuman WP, Freeny PC. Sclerosing cholangitis: CT findings. Radiology. 1988;169:635–9.
43. Tischendorf JJW, Geier A, Trautwein C. Current diagnosis and management of primary sclerosing cholangitis. Liver Transpl. 2008;14:735–46.
44. Venkatesh SK, Yin M, Ehman RL. Magnetic resonance elastography of liver: technique, analysis and clinical applications. J Magn Reson Imaging. 2013;37: 544–55.
45. Vitellas KM, Keogan MT, Freed KS, Enns RA, Spritzer CE, Baillie JM, et al. Radiologic manifestations of sclerosing cholangitis with emphasis on MR cholangiopancreatography. Radiographics. 2000;20:959–75.
46. Wiesner RH, Grambsch PM, Dickson ER, Ludwig J, MacCarty RL, Hunter EB, et al. Primary sclerosing cholangitis: natural history, prognostic factors and survival analysis. Hepatology. 1989;10:430–6.